

Structure and Bonding of the Mixed-Valent Platinum Trihalides, PtCl_3 and PtBr_3

Hans Georg von Schnering^{a,*}, Jen-Hui Chang^a, Maria Freiberg^a, Karl Peters^a, Eva-Maria Peters^a, Alim Ormeci^b, Liane Schröder^b, Gerhard Thiele^{c,*}, Caroline Röhr^c

^a Stuttgart, Max-Planck-Institut für Festkörperforschung

^b Dresden, Max-Planck-Institut für Chemische Physik fester Stoffe

^c Freiburg, Institut für Anorganische und Analytische Chemie der Albert-Ludwigs-Universität

Received August 11th, 2003.

Professor Klaus-Jürgen Range zum 65. Geburtstag gewidmet

Abstract. The isotypical crystal structures of the mixed valent trihalides PtCl_3 and PtBr_3 were redetermined by single crystal methods (space group $R\bar{3}$; trigonal setting; PtCl_3 : $a = 21.213 \text{ Å}$, $c = 8.600 \text{ Å}$, $c/a = 0.4054$; $Z = 36$; 1719 hkl; $R = 0.035$; PtBr_3 : $a = 22.318 \text{ Å}$, $c = 9.034 \text{ Å}$, $c/a = 0.4048$; $Z = 36$; 1606 hkl; $R = 0.027$). A cubic closest packing of X^- anions forms the basis of an optimized arrangement of cuboctahedrally $[\text{Pt}_6X_{12}]$ cluster molecules with Pt^{II} and enantiomers of helical chains of edge-condensed $[\text{PtX}_2\text{X}_{4/2}]$ octahedra with Pt^{IV} in *cis*- Δ - and *cis*- Λ -configuration, respectively. The bond lengths vary with the function of the X^- ligands ($\bar{d}(\text{Pt}^{II}-X) = 2.315$ and 2.445 Å ; $\bar{d}(\text{Pt}^{II}-\text{Pt}^{II}) = 3.336$

and 3.492 Å ; $d(\text{Pt}^{IV}-X) = 2.286 - 2.417 \text{ Å}$ and $2.437 - 2.563 \text{ Å}$). The Pt^{II} atoms are shifted outwards the X_{12} cuboctahedra by 0.045 Å and 0.024 Å , respectively. The symmetry governed Periodic Nodal Surface, PNS, perfectly separates the regions of different valencies. Quantum chemical calculations exclude the possible additional interactions between Pt^{II} and one of the *exo*-ligands of Pt^{IV} .

Keywords: Platinum; Platinum trihalides; Crystal structure; Electronic structure; Periodic nodal surface

Struktur und Bindung der gemischt-valenten Platin-Trihalogenide PtCl_3 und PtBr_3

Inhaltsübersicht. Die isotypen Kristallstrukturen der gemischt-valenten Trihalogenide PtCl_3 und PtBr_3 wurden an Einkristallen neu bestimmt. (Raumgruppe $R\bar{3}$; trigonale Aufstellung; PtCl_3 : $a = 21.213 \text{ Å}$, $c = 8.600 \text{ Å}$, $c/a = 0.4054$; $Z = 36$; 1719 hkl; $R = 0.035$; PtBr_3 : $a = 22.318 \text{ Å}$, $c = 9.034 \text{ Å}$, $c/a = 0.4048$; $Z = 36$; 1606 hkl; $R = 0.027$). Eine kubische Dichtestpackung der X^- -Anionen bildet die Basis einer optimierten Anordnung von kuboktaedrischen $[\text{Pt}_6X_{12}]$ -Clustermolekülen mit Pt^{II} und enantiomeren helikalen Ketten kantenkondensierter $[\text{PtX}_2\text{X}_{4/2}]$ -Oktaeder mit Pt^{IV} in *cis*- Δ - bzw. *cis*- Λ -Konfiguration. Die Bindungsängen variieren mit der

Funktion der X^- -Liganden ($\bar{d}(\text{Pt}^{II}-X) = 2.315$ bzw. 2.445 Å ; $\bar{d}(\text{Pt}^{II}-\text{Pt}^{II}) = 3.336$ bzw. 3.492 Å ; $d(\text{Pt}^{IV}-X) = 2.286 - 2.417 \text{ Å}$ bzw. $2.437 - 2.563 \text{ Å}$). Die Pt^{II} -Atome liegen um 0.045 Å bzw. 0.024 Å außerhalb der X_{12} -Kuboktaeder. Die symmetrie-bestimmte Periodische Knotenfläche, PNS, trennt perfekt die beiden Regionen unterschiedlicher Valenzen voneinander. Quantenchemische Rechnungen schließen mögliche bindende Wechselwirkungen aus, die zwischen Pt^{II} und einem der *exo*-Liganden von Pt^{IV} erwartet werden könnten.

1 Introduction

Platinum halides PtX_2 , PtX_3 and PtX_4 ($X = \text{Cl}, \text{Br}$) were synthesized and described by Wöhler et al. about 80 years

ago [1–3]. However, single crystals of the dark-red PtBr_3 and the dark-green PtCl_3 were grown by Thiele and Woditsch [4] and by Wiese et al. [5] for the first time in 1969 and 1970, respectively. The trihalides are isotypically and represent the first structural proof of the existence of distinct mixed-valent states with platinum ($\text{Pt}^{II} / \text{Pt}^{IV}$) [4, 5]. The former structure determinations based on X-ray film data [4] and 2-circle diffractometer (Philips PAILRED) data [5, 6], which don't allow a more sophisticated analysis of the structural arrangement. Furthermore, the mean bond lengths $\text{Pt}^{IV}-\text{Cl}^a$ and $\text{Pt}^{IV}-\text{Cl}^b$ listed in [5] are exchanged by mistake. A redetermination of both structures seems to be necessary to obtain reliable details with respect to possible transitions into the Pt^{III} state as observed with PtI_3 [7].

The results of new X-ray structure analyses and of quantum chemical calculations are presented here. Moreover, it

* Prof. Dr. Dr. h. c. H.G. von Schnering
Max-Planck-Institut für Festkörperforschung
Heisenbergstr. 1
D-70569 Stuttgart/Germany

* Prof. Dr. G. Thiele
Institut f. Anorg. u. Analys. Chemie
Albert-Ludwigs-Universität
Albertstraße 21
D-79104 Freiburg/Germany
e-mail: gerhard.thiele@ac.uni-freiburg.de

Table 1 Crystallographic data for PtCl_3 and PtBr_3 ^{a)}.

Formula; Mole mass	PtCl_3 ; 301.438 amu	PtBr_3 ; 434.792 amu
Crystal	dark green trigonal needle; $0.02 \times 0.02 \times 0.10$ mm	dark red trigonal needle; $0.01 \times 0.01 \times 0.08$ mm
Space group	$R\bar{3}$ (No. 148)	$R\bar{3}$ (No. 148)
Structure type; Pearson code	PtBr_3 ; $hR48$	PtBr_3 ; $hR48$
Trigonal unit cell	$a = 21.213(6) \text{ \AA}; c = 8.600(3) \text{ \AA};$ $c/a = 0.4054; V = 3351.5(3) \text{ \AA}^3; Z = 36$	$a = 22.318(9) \text{ \AA}; c = 9.034(3) \text{ \AA};$ $c/a = 0.4048; V = 3897(2) \text{ \AA}^3; Z = 36$
Rhombohedral unit cell	$a = 12.578(4) \text{ \AA}; \alpha = 114.97(1)^\circ$ $V = 1117.2(1) \text{ \AA}^3; Z = 12$	$a = 13.233(4) \text{ \AA}; \alpha = 114.980(2)^\circ$ $V = 1299.2(7) \text{ \AA}^3; Z = 12$
d_{X} ; $F(000)_{\text{hex}}$	5.377 g·cm ⁻³ ; 4644	6.670 g·cm ⁻³ ; 6588
Measurement	STOE STADI 4 Four circle diffractometer, Mo-K α , $\lambda = 0.71073 \text{ \AA}$, scintillation counter, ω -mode, $3^\circ \leq 2\theta \leq 55^\circ$. Empirical absorption correction (γ -scan); $\mu = 41.53 \text{ mm}^{-1}$	Diffractometer STOE IPDS-II, Imaging plate area detector, Mo-K α , $\lambda = 0.71073 \text{ \AA}$, $6^\circ \leq 2\theta \leq 61^\circ$. Numerical absorption correction, program SHAPE, Crystal Optimisation for Numerical Absorption Correction, Fa. STOE, Darmstadt.; $\mu = 59.86 \text{ mm}^{-1}$
Refinement	Program SHELX97 [13]; Full-matrix least squares refinement on F^2	Program SHELX97 [13]; Full-matrix least squares refinement on F^2
$N(hkl)$ meas.; unique	2091; 1719 [$R(\text{int.}) = 0.024$]	2643; 1606 [$R(\text{int.}) = 0.064$]
$N'(hkl)$ ($F^2 > 3 \sigma(F^2)$)	1679; 74 variable parameters	1606; 74 variable parameters
$R1(F)$; $R_w(F^2)$	0.035; 0.090	0.027; 0.057

Further details may be obtained from the Fachinformationszentrum Karlsruhe, Gesellschaft für wissenschaftlich-technische Zusammenarbeit, D-76344 Eggenstein-Leopoldshafen, on quoting the depositary numbers CSD-413423 (PtCl_3) and CSD-413424 (PtBr_3), the name of the authors and this journal.

Table 2 PtCl_3 : Positional and displacement parameters U_{ij}/pm^2 for the trigonal obverse setting (above; atoms at 18*f*) and for the rhombohedral setting (below; atoms at 6*f*). Displacement factor: $\exp[-2\pi^2(U_{11}h^2a^{*2} + \dots + 2U_{23}kla^*c^*)]$. Standard deviations are given in parentheses.

Atom	x	y	z	U_{11}	U_{22}	U_{33}	U_{12}	U_{13}	U_{23}
Pt1	0.00606(2)	0.09352(2)	0.15895(4)	159(2)	128(2)	184(2)	77(1)	-1(1)	-24(1)
Pt2	0.02752(2)	0.29989(2)	0.50979(4)	116(3)	109(2)	128(2)	58(1)	1(1)	-2(1)
Cl11	0.0975(2)	0.1776(2)	-0.0004(3)	224(11)	127(10)	274(14)	58(9)	32(9)	-1(9)
Cl12	0.0916(2)	0.0857(1)	0.3118(3)	236(11)	207(11)	190(11)	118(9)	-63(9)	-42(9)
Cl21	0.1153(1)	0.3854(1)	0.3428(3)	102(9)	190(10)	158(11)	50(8)	9(7)	33(8)
Cl22	0.0313(1)	0.3930(1)	0.6781(3)	207(10)	107(10)	158(13)	68(8)	38(8)	-3(8)
Cl23	0.1158(1)	0.2976(2)	0.6580(3)	195(12)	299(12)	261(14)	153(10)	-52(9)	34(10)
Cl24	0.0202(1)	0.2061(1)	0.3604(3)	258(12)	172(10)	231(11)	126(9)	-22(9)	-65(9)
Pt1	0.16501(4)	0.24641(4)	0.06543(4)	178(2)	157(2)	192(2)	127(2)	145(2)	141(2)
Pt2	0.53731(4)	0.78216(4)	0.20990(4)	127(2)	122(2)	126(2)	94(2)	96(2)	96(2)
Cl11	0.0972(4)	0.0797(4)	-0.1780(4)	289(14)	243(13)	247(13)	195(12)	226(12)	200(12)
Cl12	0.4033(4)	0.3059(4)	0.2261(4)	150(10)	210(11)	225(11)	119(10)	126(10)	164(10)
Cl21	0.4581(3)	0.6129(3)	-0.0427(3)	155(10)	183(11)	138(10)	133(10)	111(10)	101(10)
Cl22	0.7093(3)	0.0398(3)	0.2851(3)	196(12)	130(11)	151(12)	103(11)	133(11)	108(11)
Cl23	0.7738(4)	0.8398(4)	0.3605(4)	209(12)	314(15)	242(13)	220(12)	154(11)	208(12)
Cl24	0.3806(4)	0.5463(4)	0.1542(4)	219(11)	188(11)	270(12)	141(10)	183(10)	189(10)

will be shown that the appropriate symmetry governed Periodic Nodal Surface, PNS, separates the regions of Pt^{II} and Pt^{IV} in a natural way.

2 Synthesis and Properties

Since 1970 the preparation, the thermal decomposition and the growth of platinum halide crystals from the vapor phase was studied by several groups intensely [4, 5, 8–12]. The reaction of platinum metal with halogens is strongly inhibited by the formation of surface layers [10]. Therefore, the conventional method for the preparation of the tetrahalides is the thermal decomposition of commercial products of hexahalogenoplatinum(IV) acids $\text{H}_2\text{PtX}_6 \cdot x\text{H}_2\text{O}$ in a stream of N_2/Cl_2 resp. N_2/Br_2 ($T \approx 500 \text{ K}$, 2–3 hours, quartz glass tube, corundum crucible) [9]. Powder samples of the trihalides are obtained by thermal decomposition of the tetrahalides in closed quartz glass ampoules with presence of halogens (Pressure $X_2 \geq 1 \text{ bar}$, $T \approx 675 \text{ K}$) [9].

When PtBr_4 was heated in a quartz ampoule for 5 days in a 900 K / 520 K temperature gradient, black needle-shaped single crystals of PtBr_4 were found at the 520 K zone, in contact with dark green trigonal needles of PtBr_3 crystals in the 650 K zone [8]. Single crystals of the homogeneous trihalides PtCl_3 and PtBr_3 can be prepared by transport methods [4, 5, 12], in particular with Al_2X_3 as a transporting agent [10]. Noticeable is the brass-colored reflectivity of the trigonal prism faces of PtX_3 crystals. PtCl_3 is diamagnetic ($-66 \cdot 10^{-6} \text{ cm}^3 \cdot \text{mol}^{-1}$ [5]) and PtBr_3 shows a very low paramagnetism ($150 \cdot 10^{-6} \text{ cm}^3 \cdot \text{mol}^{-1}$ [4]).

3 Structure Determination

The crystallographic data are collected in Table 1, Table 2 and Table 3. We take the former parameters of PtBr_3 [4] and PtCl_3 [5, 6] as starting values.

Table 3 PtBr₃: Positional and displacement parameters U_{ij}/pm² for the trigonal obverse setting (*above*; atoms at 18*f*) and for the rhombohedral setting (*below*; atoms at 6*f*). Displacement factor: exp[-2π²(U₁₁h²a*²+...+2U₂₃klb*c*)]. Standard deviations are given in parentheses.

Atom	x	y	z	U ₁₁	U ₂₂	U ₃₃	U ₁₂	U ₁₃	U ₂₃
Pt1	0.00705(3)	0.09351(4)	0.1582(1)	160(3)	130(3)	110(9)	76(2)	-7(3)	-19(3)
Pt2	0.02723(3)	0.29961(4)	0.5076(1)	126(3)	114(3)	85(7)	63(2)	5(3)	-2(3)
Br11	0.0992(1)	0.1783(1)	-0.0009(2)	206(9)	144(8)	191(21)	60(7)	9(9)	-5(9)
Br12	0.0927(1)	0.0858(1)	0.3129(3)	215(9)	209(9)	141(25)	105(8)	-52(10)	-35(9)
Br21	0.1166(1)	0.3855(1)	0.3419(3)	119(8)	172(9)	162(18)	52(7)	2(9)	53(9)
Br22	0.0310(1)	0.3943(1)	0.6743(3)	202(8)	109(7)	152(19)	52(7)	41(10)	-12(9)
Br23	0.1173(1)	0.2978(1)	0.6569(3)	225(9)	274(11)	228(20)	160(8)	-25(11)	35(10)
Br24	0.0201(1)	0.2035(1)	0.3579(3)	274(10)	178(9)	145(21)	134(8)	14(9)	-55(9)
Pt1	0.1653(1)	0.2447(1)	0.0647(1)	114(7)	106(7)	128(7)	68(7)	82(7)	83(7)
Pt2	0.5348(1)	0.7800(1)	0.2080(1)	96(6)	84(6)	92(6)	57(6)	61(6)	58(6)
Br11	0.0983(3)	0.0782(3)	-0.1793(3)	200(18)	187(17)	186(18)	129(17)	151(17)	138(17)
Br12	0.4056(3)	0.3060(3)	0.2271(3)	114(20)	166(20)	180(21)	82(20)	90(20)	117(20)
Br21	0.4585(3)	0.6107(3)	-0.0436(3)	156(16)	206(17)	123(15)	141(15)	104(14)	111(15)
Br22	0.7053(3)	0.0377(3)	0.2800(3)	192(16)	130(16)	145(15)	97(15)	131(15)	99(15)
Br23	0.7742(3)	0.8375(3)	0.3591(3)	208(18)	265(17)	209(17)	189(17)	135(17)	176(17)
Br24	0.3780(3)	0.5413(3)	0.1545(3)	178(18)	99(17)	193(19)	73(17)	121(18)	106(18)

4 Calculation of Periodic Nodal Surfaces, PNS

The Periodic Nodal Surfaces, PNS, are structure invariant space partitioners, solely determined by symmetry [14]. The calculation as nodes of simple Fourier series and the use of PNS to analyze the generalized organization of crystal structures is described manifold [15–25]. The symmetry of PtCl₃ and PtBr₃ is R3} and the axial ratio amounts c/a = 0.405 (trigonal setting). This small c/a ratio shifts the reciprocal lattice point (110) closest to the origin, followed by (101) with the same multiplicity (n = 6). We take |S(110)| = |S(101)| = 1 and α(110) = α(101) = 0 as Fourier coefficients, for simplicity. These amplitudes |S| and phase angles α are identical for the space groups R3} and R3}m and, therefore, the generating and resulting symmetry is the same. The squares of the reciprocal lengths are in the ratio [sin²θ(110) / sin²θ(101)] ≈ 0.5, which will be used as decay factor φ (see Equ. (1)). The appropriate PNS will now be calculated according to R3}m<(110)⁰, (101)⁰>R3}m [14] which includes the symmetry equivalent coefficients (110), (210), (120) and (101), (111), (011), respectively. The rearrangement yields in (cX = cos 2πx etc.):

$$[c(X+Y) + c(-2X+Y) + c(X-2Y)] + \\ \varphi[c(X+Z) + c(-X+Y+Z) + c(-Y+Z)] = 0 \quad (1)$$

with φ = 0.5 (see above).

Fig. 1 shows the PNS. It is easily to realize that the first part of Equ. (1) results in a hexagonal packing of cylinders with R_{cyl} = 0.1904·a_{hex}. The second part modulates the cylinders along c_{hex}. The space will be divided into two different labyrinth types, namely around the lattice complex R2z [26] in the cylinders and around the two equivalent lattice complexes (M + 00¹/₂M) outside the cylinders. In the rhombohedral setting the lattice complexes are P2xxx and (J + 1/2¹/₂1/2J), which immediately show the relations to the non-isomorphic supergroup Im3m with the lattice complexes I and J*.

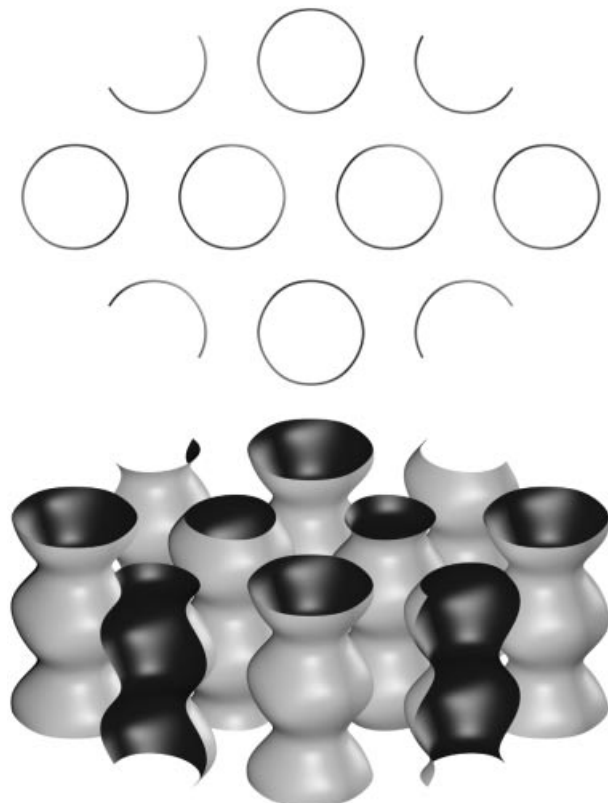


Fig. 1 Periodic Nodal Surface PNS ($P2xxx \wedge J + 1/2^1/2^1/2J$), which divides the space into two different labyrinths. The modulated cylinders envelope the lattice complex R2z (or P2xxx) [26]. The larger labyrinth contains the two lattice complexes M and 00¹/₂M (or J + 1/2¹/₂1/2J).

Again, we would like to draw the reader's attention to the studies of Andersson et al. [27] about the representation of such surfaces in exponential scale. Finally, Andersson and Jacobs [28–30] have discovered relations of general importance in the mathematics of continuum, which show surpris-

ing analogies between mathematical and chemical structures.

5 Quantum Mechanical Calculations

We used the tight-binding linear muffin-tin orbitals (TB-LMTO) method within the atomic-sphere approximation (ASA) [31, 32] to perform first-principles electronic structure calculations on PtCl_3 and PtBr_3 . The calculations were scalar-relativistic and the combined correction term was included. Local density approximation (LDA) to the density functional theory [33] was utilized through the exchange-correlation potential due to von Barth and Hedin [34]. The valence states are chosen as follows: Cl: 3p, 4s, 3d (last two are downfolded [35]); Br: 4p, 5s, 4d (last two downfolded); Pt: 6s, 6p, 5d, 5f (last one downfolded). Since the crystal structure is quite an open one, *cf.* the packing ratio is about 25 %, interstitial (empty) spheres had to be inserted for a proper representation of charge density in the whole unit cell. The positions and radii of these spheres were determined by an automatic algorithm [32]. Brillouin zone (BZ) integrations were done by the tetrahedron method [36]; 117 tetrahedra were used in the irreducible BZ. In order to elucidate the bonding properties we generated the contour plots of the charge density and the Electron Localization Function (ELF) [37].

6 Results and Discussion

6.1 Crystal Structure

The mixed-valent PtCl_3 and PtBr_3 form the PtBr_3 type of structure [4] which represents a well optimized arrangement of Pt_6X_{12} cluster molecules with Pt^{II} ($\text{X} = \text{Cl}, \text{Br}$) and helical chains of edge-condensed PtX_6 octahedra $\text{Pt}^{\text{IV}}[\text{PtX}_2\text{X}_{4/2}]$ with Pt^{IV} , forming two enantiomers ($3_1, 3_2$ screws). The chirality is implanted in the *cis*- Δ -configuration and the *cis*- Λ -configuration of the condensed octahedra, respectively. The common edges act formally as η^2 -chelate ligands (Fig. 2). One type forms the helices around the 3_1 screw axes and the other type goes around the 3_2 screw axes. This arrangement is quite different from the chains in PtI_4 [38] and PtBr_4 [8] where the two configurations alternate by glide plane operations. The volumes of PtCl_3 and PtBr_3 are slightly smaller than the mean volumes of PtX_2 and PtX_4 (0.99 and 0.97).

The 108 X atoms per trigonal unit cell form the pattern of a cubic closest packing. Each of the three layers parallel (001) at $z = 0, 1/3, 2/3 (\pm 0.02)$ contains 36 X atoms and the defect \square in the Pt_6X_{12} cluster center (Fig. 3), corresponding with the 36 nodes (without \square) of a $3^4 \cdot 6 + 3^6$ (6:30) net and with 37 nodes (including \square) of a uniform 3^6 net, respectively. The edge length of a homogeneous 3^6 net is $a' = a_{\text{hex}}(37)^{-1/2}$ and, therefore, the positional parameters at $z = 0$ will be $x, y = n/37$ ($n = \text{integer}$). With respect to the rhombohedral symmetry of the trigonal structure the parameters of Table 2 and Table 3 have to be compared

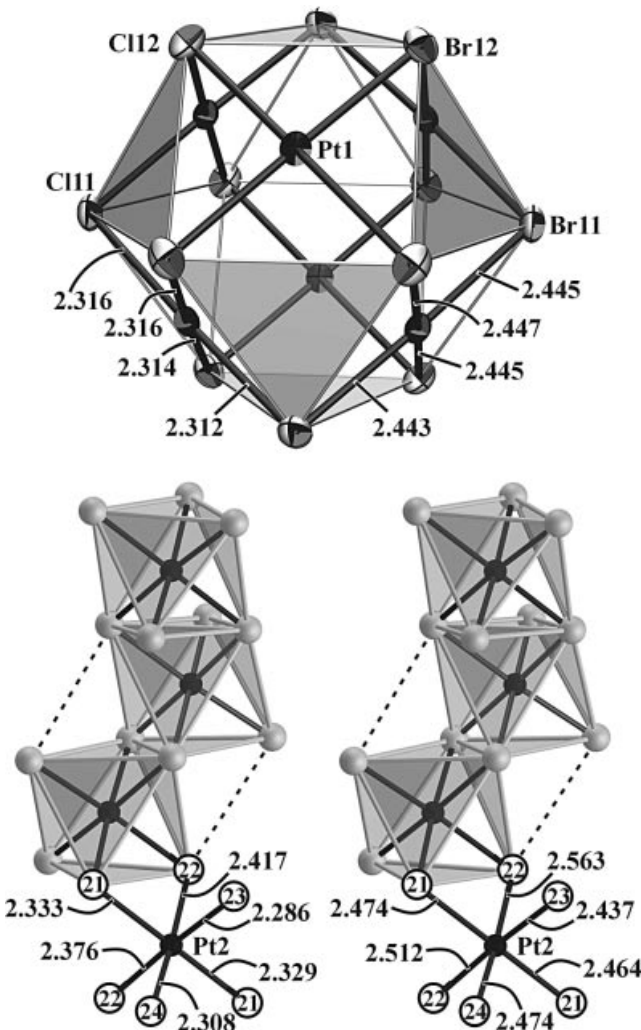


Fig. 2 The $\text{Pt}_6^{\text{II}}\text{X}_{12}$ cluster molecule (above) and one of the enantiomeric helices of edge-condensed $\text{Pt}^{\text{IV}}[\text{PtX}_2\text{X}_{4/2}]$ octahedra in *cis*- Δ -configuration (below). The atomic labeling and the $\text{Pt}-\text{X}$ bond lengths $d/\text{\AA}$ are indicated (Table 4). The dotted lines show the short van der Waals contacts which result from the formation of the helix. (left: $\text{X} = \text{Cl}$; right: $\text{X} = \text{Br}$).

with multiples $x, y = m/111$ ($m = \text{integer}$): $\text{X}11$ (12; 21), $\text{X}12$ (11; 10), $\text{X}21$ (13; 43), $\text{X}22$ (4; 44), $\text{X}23$ (13; 32), $\text{X}24$ (2; 22). The small distortions of the ideal 3^6 net (Fig. 3) results from contractions of the Pt_6X_{12} cluster and of the PtX_4 -screws as well as from different functions of the halide ligands. The axial ratio of the ideal 3^6 net ($c/a' = 2.466$) shows that the deviation of a cubic closest packing is very small ($\sqrt{6} = 2.4495$).

The structure invariant Periodic Nodal Surface PNS ($P2\text{xxx} \wedge J + 1/2^{1/2} 1/2 J$) separates perfectly the dihalide regions from the tetrahalide regions of the mixed-valent trihalide structures (Fig. 4). There is an interesting relation between the structures of PtCl_3 and $\beta\text{-PtCl}_2$ ($\text{Pt}_6\text{Cl}_{12}$) [39]. Both base on cubic closest packed anion arrays with very similar trigonal c-axes (8.60 \AA ; 8.66 \AA) but very different trigonal a-axes. Each anion layer contains per unit cell 13 X positions in $\beta\text{-PtCl}_2$ but 37 X positions in PtCl_3 . This

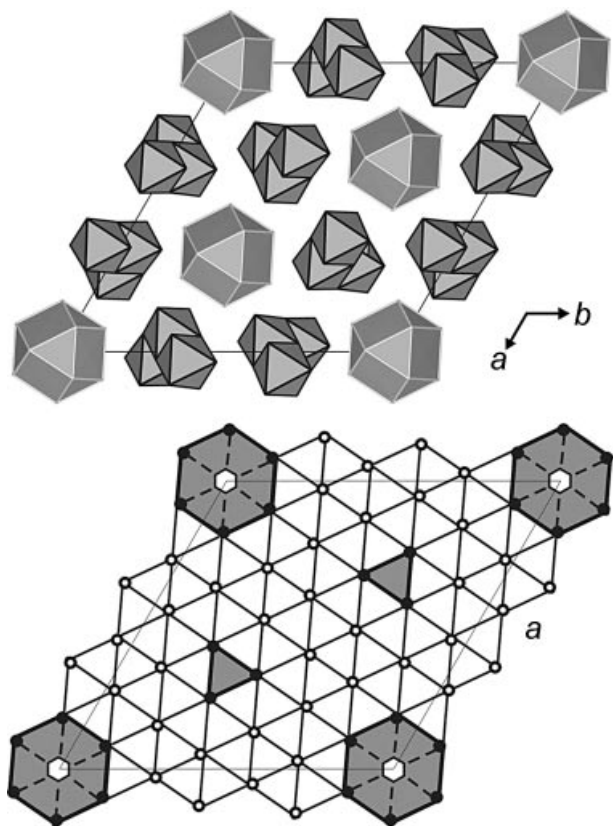


Fig. 3 View of the PtCl_3 (PtBr_3) structure down the trigonal c-axis (above) and the 3^6 net of 37 nodes in the plane at $z = 0 \pm 0.02$ ($36 \text{ X} + 1 \square$) (below). The ideal 3^6 net with the positions $x, y = n/37$ is outlined. The real X positions are shown by open circles. Shaded areas belong to atoms X_{11} and X_{12} forming the Pt_6X_{12} cluster. It is seen that the helices of condensed octahedra are threaded through a formerly body-centered cubic arrangement of Pt_6X_{12} clusters (see Text).

results in a nearly perfect body centered cubic structure of $[\text{Pt}_6\text{Cl}_{12}]$ clusters [39], where the trigonal c-axis represents half of the cubic space diagonal. This direction is characterized by columns of clusters separated by trigonal X_6 anti-prisms. These columns are unchanged present in PtCl_3 (Fig. 4) but now separated by the PtCl_4 spirals threaded through the trigonal basis. It is a nice idea to think that PtCl_3 is formed from PtCl_2 by diffusion of PtCl_4 chains through the expanding (001) plane along the c-axis.

6.2 Molecular Structure

Important bond lengths and interatomic distances are collected in Table 4. The shape of the $[\text{Pt}_6\text{Cl}_{12}]$ cluster of Pt^{II} is almost unchanged with respect to the dichloride cluster [39], including the small trigonal stretching. The mean bond lengths are $\bar{d}(\text{Pt}^{\text{II}}-\text{Cl}^{\text{i}}) = 2.315 \text{ \AA}$ and $\bar{d}(\text{Pt}^{\text{II}}-\text{Br}^{\text{i}}) = 2.445 \text{ \AA}$. The mean (nonbonding) intra-cluster $\text{Pt}^{\text{II}}-\text{Pt}^{\text{II}}$ distances are 3.336 \AA and 3.492 \AA , respectively. Together with the empty cluster center \square , the X_{12}^i cubooctahedra form nuclei of cubic closest packings with $\bar{d}(\text{Cl}^{\text{i}}-\text{Cl}^{\text{i}}) = 3.273 \text{ \AA}$

and $\bar{d}(\text{Br}^{\text{i}}-\text{Br}^{\text{i}}) = 3.458 \text{ \AA}$. These distances are substantial shorter than derived from the 'ideal' unit cell packings ($a(37)^{-1/2} = 3.487 \text{ \AA}$ and 3.669 \AA ; see above). The differences are compensated by the larger van der Waals distances to the enveloping neighbor units (3.68 \AA and 3.85 \AA). The Pt^{II} atoms are shifted outwards of the clusters by 0.045 \AA and 0.024 \AA , respectively. These values correspond with those of the hexameric dihalides [39] and, they indicate that no additional interactions may be present with the larger distant *exo*- X_{24} ligands of Pt^{IV} (2.842 \AA and 2.940 \AA ; Table 4; see below).

The distortions in the octahedral Pt^{IV} coordination mainly result from four effects: (i) the different functions of the single-bonded X^{e} *exo*-ligands and the bridging X^{b} ligands (Fig. 2, Table 4); (ii) the *cis*-configuration of the two X^{e} ligands; (iii) the internal tension in the center of the helices; (iv) relatively short intermolecular distances between neighboring helices (Fig. 3). Therefore, the ratio $\bar{d}(\text{Pt}^{\text{IV}}-\text{X}) / (\bar{d}(\text{Pt}^{\text{II}}-\text{X}) = 1.12-1.17$ is somewhat larger than in the pairs $\text{PtX}_6^{2-}/\text{PtX}_4^{2-}$. The bond lengths of the single-bonded X^{e} *exo*-ligands correspond with the covalent radii sums ($\bar{d}(\text{Pt}^{\text{IV}}-\text{Cl}^{\text{e}}) = 2.297 \text{ \AA} \triangleq 2.29 \text{ \AA}$ and $\bar{d}(\text{Pt}^{\text{IV}}-\text{Br}^{\text{e}}) = 2.456 \text{ \AA} \triangleq 2.44 \text{ \AA}$), but the twofold bonded X^{b} bridging ligands are closer bonded as expected for Pauling Bond Order PBO = $1/2$ ($\bar{d}(\text{Pt}^{\text{IV}}-\text{Cl}^{\text{b}}) = 2.364 \text{ \AA} < 2.47 \text{ \AA}$ and $\bar{d}(\text{Pt}^{\text{IV}}-\text{Br}^{\text{b}}) = 2.504 \text{ \AA} < 2.62 \text{ \AA}$). Furthermore, the lengths of the two *exo*-bonds as well as the two types of $\text{Pt}^{\text{IV}}-\text{X}^{\text{b}}$ bonds are different. This demonstrates together with the irregular intra-polyhedral $\text{X}-\text{X}$ contacts the substantial internal tension of the helices. Helices of *regular* edge-condensed octahedra yields in *intra*-octahedral and *inter*-octahedral $\text{X}-\text{X}$ distances of the same lengths. In the real structure these two types have to act as intramolecular ones (strongly influenced by the $\text{Pt}-\text{X}$ bonds) and as intermolecular ones of the van der Waals type (dotted lines in Fig. 2). To realize this, the central part of the helix became irregular with respect to all interatomic distances (X_{22} atoms) including the shift of the *exo*- X_{24} atoms from Pt^{IV} toward Pt^{II} .

An analysis of the deviations of the real structure from an idealized c.c.p. anion pattern shows (Fig. 3, Fig. 4):

(1) One starts with a c.c.p. X-array with $c/a' = \sqrt{6}$ and contracts the $[\text{Pt}_6\text{X}_{12}]$ cluster and the $[\text{PtX}_2\text{X}_{4/2}]$ octahedra to fit the observed ratio $\bar{d}(\text{X}-\text{X})_{\text{intra}} / \bar{d}(\text{X}-\text{X})_{\text{inter}} = 0.89$.

(2) It is seen that non-acceptable ($\text{X}-\text{X}$)_{inter} distances occur in the helices (X_{22} contacts; see above) and also between adjacent helices.

(3) To overcome the intra-helical ones, the helices has to be stretched and, for the intra-helical ones the *cis*- Δ - and *cis*- Λ -helices has to be shifted along [001] alternating by $\pm 0.08 \text{ \AA}$ and $\pm 0.07 \text{ \AA}$, respectively (see $z(\text{Pt}2)$ in Table 2 and Table 3). Both effects are seen in the real structures. In that way the shortest *inter*-molecular $\text{X}-\text{X}$ distances will be expanded from 3.44 \AA to 3.58 \AA (PtCl_3) and from 3.52 \AA to 3.64 \AA (PtBr_3).

(4) In the idealized PtCl_3 structure according to (2), the above discussed $\text{Pt}^{\text{II}}-\text{Cl}_{24}$ distance is shorter (2.77 \AA) than

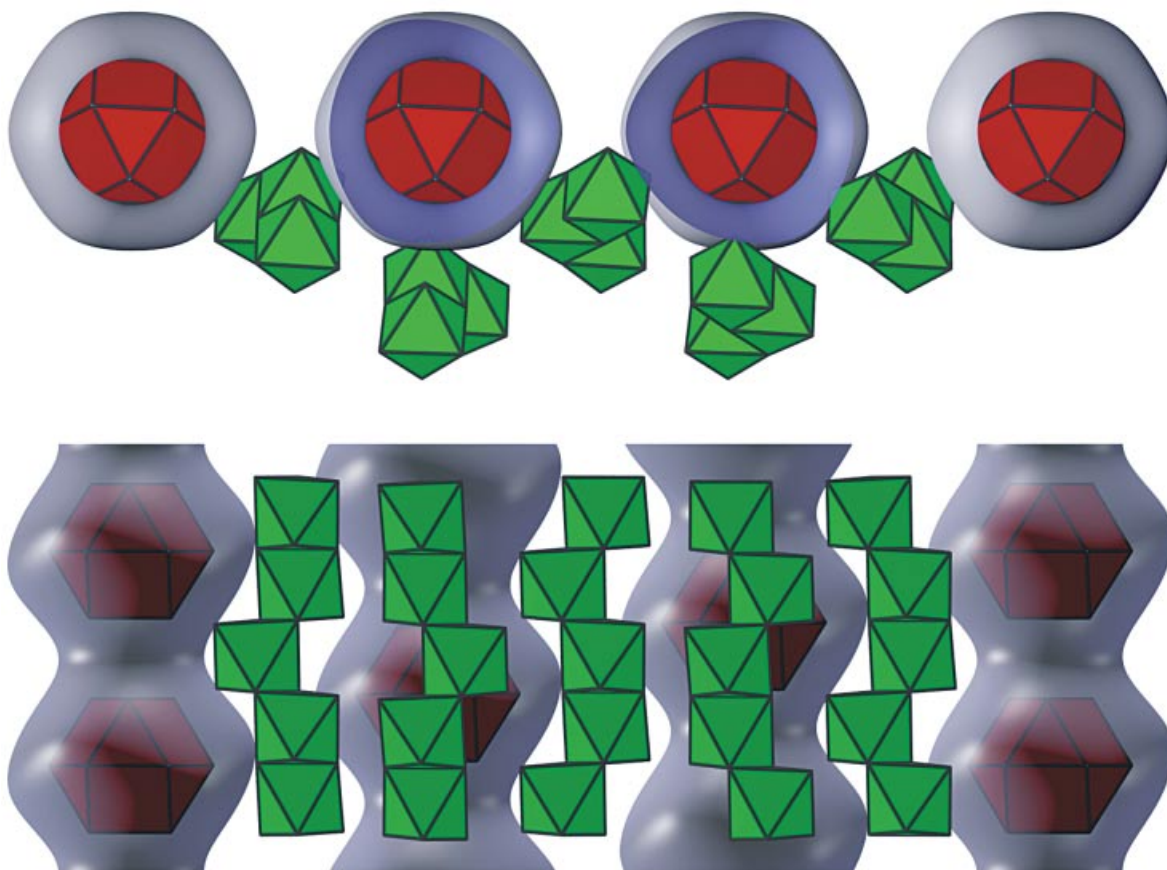


Fig. 4 The PNS ($P2xxx \wedge J + 1/2 1/2 1/2 J$) separates perfectly the region of $\text{Pt}_6^{\text{II}}\text{X}_{12}$ clusters from the region of $[\text{Pt}^{\text{IV}}\text{X}_2\text{X}_{4/2}]$ helices. The helices climb along the modulations of three neighboring cylinders and extend the single-bonded *exo*-ligands X24 toward the waists (see text).

Table 4 Selected interatomic distances d/ \AA (Standard deviation); n = multiplicity per atom. i = inner ligand; b = bridging ligand; e = exo-ligand

Atoms	$[\text{PtX}_1^i]_{12}$ cluster; Pt(II)				$[\text{PtX}_{4/2}^6\text{X}_5^e]$ helix; Pt(IV)				Atoms	n	X–X distances						
	n	X = Cl	X = Br	Atoms	n	X = Cl	X = Br	function			intramolecular	intermolecular	n				
Pt1	–	X11	1	2.316(3)	2.445(2)	Pt2	–	X21	1	2.329(2)	2.464(2)	peripheral X ^b	Cl ⁱ – Cl ⁱ	4	3.261 – 3.283	3.556 – 3.810	7
	–	X11	1	2.316(3)	2.447(2)	–	X21	1	2.333(2)	2.474(2)	Br ⁱ – Br ⁱ	4	3.450 – 3.468	3.715 – 3.977	7		
	–	X12	1	2.312(3)	2.443(2)	–	X22	1	2.376(2)	2.512(3)	Cl ^b – Cl	7	3.218 – 3.525	3.581 – 3.805	5		
	–	X12	1	2.314(3)	2.445(2)	–	X22	1	2.417(2)	2.563(3)	central X ^b	Br ^b – Br	7	3.436 – 3.644	3.644 – 3.953	5	
	–	X24	1	2.842(3)	2.940(3)	–	X23	1	2.286(3)	2.437(2)		Cl ^e – Cl	4	3.240 – 3.319	3.524 – 3.810	8	
	Pt1	–	Pt1	2	3.330(1)	3.487(2)	–	X24	1	2.308(3)	2.474(2)	Br ^e – Br	4	3.445 – 3.539	3.644 – 3.977	8	
	Pt1	–	Pt1	2	3.342(1)	3.496(2)	Pt2	–	Pt2	2	3.463(1)	3.640(1)	□ – X ⁱ	12	3.273 (Cl); 3.458 (Br)		

in the real structure (2.842 \AA), which may also be taken as an argument against additional bonding interaction (see below).

6.3 Quantum Chemical Results

In the $\text{Pt}_6\text{Cl}_{12}$ structure (β - PtCl_2) empty trigonal Cl_6 prisms cover the square-planar PtCl_4 fragments of the cluster to give space for the extended (antibonding) electron clouds of Pt^{II} [39]. Now, in the structures of PtCl_3 and PtBr_3 this space is 'closed' by the X24 atoms, even if the $\text{Pt}^{\text{II}}\text{–X24}$ distances are very large (2.842 \AA and 2.940 \AA). Nevertheless, these distances may correspond with bond orders of

about 0.15. Furthermore, the X24 *exo*-ligands show weaker $\text{Pt}^{\text{IV}}\text{–X}^e$ bonds than the X23 *exo*-ligands (Table 4), which also may indicate weak additional $\text{Pt}^{\text{II}}\text{–X24}$ interactions. On the other hand, the topological analysis has shown (see above) that the change in the $\text{Pt}^{\text{IV}}\text{–X}^e$ bonds primarily results from sterical reasons.

Indeed, the quantum chemical calculations give no indication of significant bonding interactions. The most important ELF section of the $[\text{Pt}_6\text{Cl}_{12}]$ clusters is shown in Fig. 5.

This section includes the cluster center, two Pt^{II} atoms (Pt1), the inner ligand X12 and the surrounding X24 li-

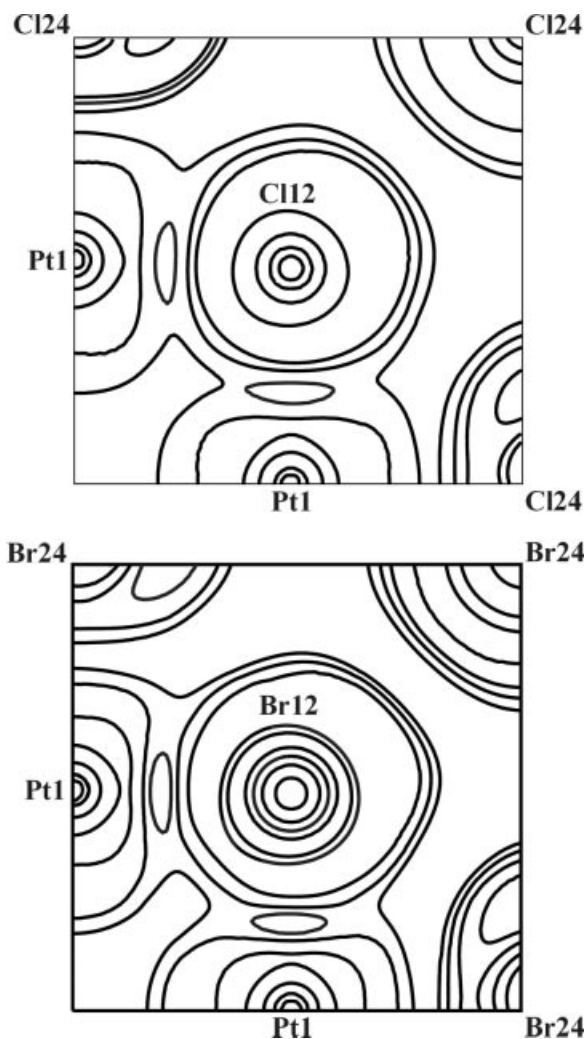


Fig. 5 Section of the Electron Localisation Function, ELF, through the Pt_6X_{12} clusters. The plane is defined by the empty cluster center \square at $x = y = 0$ and by the two Pt1 atoms (x horizontal; y vertical). The ELF-isolines are equidistant on an arbitrary scale.

gands of Pt^{IV} (Pt2) (X12 and X24 are not exactly in the $\text{Pt1}-\square-\text{Pt1}$ plane). It is seen that the extended electron cloud of Pt^{II} along the x, y-axes is not as large as in the $\text{Pt}_6\text{Cl}_{12}$ single molecule [39], but is still present. The internal $\text{Pt1}-\text{X}12$ bonds are clearly represented as ELF bridges. On the other hand, the orientation of the extended lone pair electron distribution of the X24 atoms (which represents the real donor properties of the *exo*-ligands X24) is oriented *perpendicular* to the $\text{Pt1}-\text{X}24$ direction and is separated from Pt1 by an ELF-valley. In other words, there is obviously no $\text{Pt}^{\text{II}}-\text{X}^{\text{e}}$ interaction present.

Acknowledgment. This work was supported by the Fonds der Chemischen Industrie. The Max-Planck-Gesellschaft supports one of us (J.-H. C.) by a scholarship.

References

- [1] L. Wöhler, F. Martin, *Ber. Dtsch. Chem. Ges.* **1909**, *42*, 3958.
- [2] L. Wöhler, S. Streicher, *Ber. Dtsch. Chem. Ges.* **1913**, *46*, 1591.
- [3] L. Wöhler, F. Müller, *Z. Anorg. Allg. Chem.* **1925**, *149*, 377.
- [4] G. Thiele, P. Woditsch, *Angew. Chem.* **1969**, *81*, 706; *Angew. Chem. Int. Ed. Engl.* **1969**, *8*, 672.
- [5] U. Wiese, H. Schäfer, H. G. von Schnerring, C. Brendel, K. Rinke, *Angew. Chem.* **1970**, *82*, 135; *Angew. Chem. Int. Ed. Engl.* **1970**, *9*, 158; U. Wiese, *Dissertation*, Univ. Münster, **1970**.
- [6] H. G. von Schnerring, U. Wiese, K. Peters, H. Schäfer, unpublished crystal data and parameters of the PtCl_3 structure, **1970**.
- [7] G. Thiele, M. Steiert, D. Wagner, H. Wochner, *Z. Anorg. Allg. Chem.* **1984**, *516*, 207.
- [8] P. Woditsch, *Dissertation* Univ. Erlangen-Nürnberg **1969**.
- [9] M. Degner, B. Holle, J. Kamm, M.F. Pilbrow, G. Thiele, D. Wagner, W. Weigl, P. Woditsch, *Transition Met. Chem.* **1975**, *76*, *1*, 41.
- [10] H. Schäfer, U. Wiese, C. Brendel, J. Nowitzki, *J. Less-Common Met.* **1980**, *76*, 63–72.
- [11] W. Gerhardt, H. Schäfer, *Z. Anorg. Allg. Chem.* **1985**, *530*, 227.
- [12] E. Schönher, M. Wojnowski, A. Rabenau, S. Lacher, *J. Less-Common Met.* **1988**, *137*, 277.
- [13] G. M. Sheldrick, Program Package SHELLXTL-plus. Release 5.1. Bruker Analytical X-Ray Instruments Inc., Copyright **1998**.
- [14] H. G. von Schnerring, R. Nesper, *Z. Phys. B-Condensed Matter* **1991**, *83*, 407.
- [15] H. G. von Schnerring, M. Oehme, G. Rudolf, *Acta Chem. Scand.* **1991**, *45*, 873.
- [16] Yu. Grin, U. Wedig, H. G. von Schnerring, *Angew. Chem.* **1995**, *107*, 1318; *Angew. Chem. Int. Ed. Engl.* **1995**, *34*, 1204.
- [17] Yu. Grin, U. Wedig, F. Wagner, H. G. von Schnerring, A. Savin, *J. Alloys Comp.* **1997**, *255*, 203.
- [18] Yu. Grin, A. Zürn, L. Schröder, H. G. von Schnerring, *Beziehungen zwischen Periodischen Knotenflächen und Graphen*, Abstract zur Tagung Theoretische Kristallographie, Hünfeld, **1996**.
- [19] A. Zürn, *Dissertation*, Univ. Stuttgart, **1998**.
- [20] H. G. von Schnerring, *Nova Acta Leopoldina*, Halle (Saale), **1991**, *N. F.* *65*, Nr. 277, 89.
- [21] H. G. von Schnerring, R. Nesper, *J. Physique, Colloq. C7*, **1990**, 393; *Angew. Chem.* **1986**, *98*, 111; *Angew. Chem. Int. Ed. Engl.* **1986**, *25*, 110; *Angew. Chem.* **1987**, *99*, 1097; *Angew. Chem. Int. Ed. Engl.* **1987**, *26*, 1059.
- [22] M. Somer, U. Herterich, J. Čurda, W. Carrillo-Cabrera, A. Zürn, K. Peters, H. G. von Schnerring, *Z. Anorg. Allg. Chem.* **2000**, *626*, 625.
- [23] R. Nesper, S. Leoni, *Chem. Phys. Chem.* **2001**, *2*, 413.
- [24] S. Leoni, R. Nesper, *Acta Crystallogr.* **2000**, *A56*, 383.
- [25] E. Irran, K. Kollisch, S. Leoni, *Chem. Eur. J.* **2000**, *6*, 2714.
- [26] T. Hahn, (Edit.), *International Tables for Crystallography*, Vol. A, 2nd revised Edition, Kluwer Academic Publ. Dordrecht, **1996**.
- [27] S. Andersson, M. Jacob, S. Lidin, *Z. Kristallogr.* **1995**, *201*, 3; *Z. Kristallogr.* **1995**, *210*, 315; *Z. Kristallogr.* **1995**, *210*, 826.
- [28] S. Andersson, M. Jacob, *The Mathematics of Structures*, R. Oldenbourg Verlag, München, **1997**.
- [29] M. Jacob, S. Andersson, *The nature of mathematics and the mathematics of nature*, Elsevier, Amsterdam, **1998**.
- [30] S. Andersson, K. Larsson, M. Larsson, M. Jacob, *Biomathematics*, Elsevier, Amsterdam, **1999**.
- [31] O. K. Andersen, *Phys. Rev.* **1975**, *B12*, 3060; O.K. Andersen, O. Jepsen, *Phys. Rev. Lett.* **1984**, *53*, 2571; O. Jepsen, O. K. Andersen, *Z. Phys.* **1995**, *B97*, 35.

- [32] O. Jepsen, O. K. Andersen, The Stuttgart TB-LMTO-ASA program, version 47; Max-Planck-Institut für Festkörperforschung, Stuttgart.
- [33] P. Hohenberg, W. Kohn, *Phys. Rev.* **1964**, *B136*, 864; W. Kohn, L. J. Sham, *Phys. Rev.* **1965**, *A140*, 1133.
- [34] U. von Barth, L. Hedin, *J. Phys.* **1971**, *C4*, 2064.
- [35] W. R. L. Lambrecht, O.K. Andersen, *Phys. Rev.* **1986**, *B34*, 2439.
- [36] O. Jepsen, O. K. Andersen, *Solid State Commun.* **1971**, *9*, 1763; P.E. Blöchl, O. Jepsen, O. K. Andersen, *Phys. Rev.* **1994**, *B49*, 16223.
- [37] A. D. Becke, K. E. Edgecombe, *J. Chem. Phys.* **1990**, *92*, 5397.
- [38] K. Brodersen, G. Thiele, B. Holle, *Z. Anorg. Allg. Chem.* **1969**, *369*, 154.
- [39] H. G. von Schnering, J.-H. Chang, K. Peters, E.-M. Peters, F. R. Wagner, Yu. Grin, G. Thiele, *Z. Anorg. Allg. Chem.* **2003**, *629*, 516.